

# Elemental Mercury Concentrations and Fluxes in the Tropical Atmosphere and Ocean

Anne L. Soerensen,<sup>\*,†,‡</sup> Robert P. Mason,<sup>§</sup> Prentiss H. Balcom,<sup>§</sup> Daniel J. Jacob,<sup>‡</sup> Yanxu Zhang,<sup>‡</sup> Joachim Kuss,<sup>||</sup> and Elsie M. Sunderland<sup>†,‡</sup>

<sup>†</sup>Department of Environmental Health, Harvard School of Public Health, Boston, Massachusetts 02215, United States

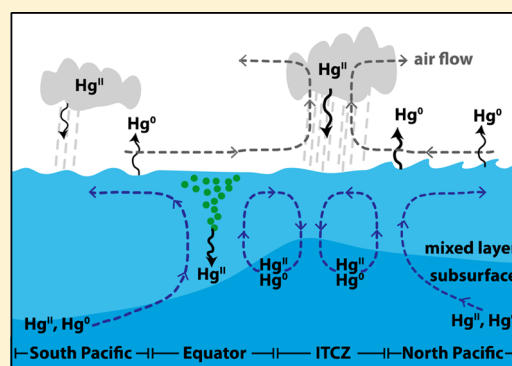
<sup>‡</sup>School of Engineering and Applied Sciences, Harvard University, Cambridge, Massachusetts 02138, United States

<sup>§</sup>Department of Marine Sciences, University of Connecticut, 1080 Sennecossett Road, Groton, Connecticut 06340, United States

<sup>||</sup>Department of Marine Chemistry, Leibniz Institute for Baltic Sea Research, 18119 Rostock, Germany

## Supporting Information

**ABSTRACT:** Air–sea exchange of elemental mercury ( $\text{Hg}^0$ ) is a critical component of the global biogeochemical Hg cycle. To better understand variability in atmospheric and oceanic  $\text{Hg}^0$ , we collected high-resolution measurements across large gradients in seawater temperature, salinity, and productivity in the Pacific Ocean ( $20^\circ\text{N}$ – $15^\circ\text{S}$ ). We modeled surface ocean Hg inputs and losses using an ocean general circulation model (MITgcm) and an atmospheric chemical transport model (GEOS-Chem). Observed surface seawater  $\text{Hg}^0$  was much more variable than atmospheric concentrations. Peak seawater  $\text{Hg}^0$  concentrations ( $\sim 130$  fM) observed in the Pacific intertropical convergence zone (ITCZ) were  $\sim 3$ -fold greater than surrounding areas ( $\sim 50$  fM). This is similar to observations from the Atlantic Ocean. Peak evasion in the northern Pacific ITCZ was four times higher than surrounding regions and located at the intersection of high wind speeds and elevated seawater  $\text{Hg}^0$ . Modeling results show that high Hg inputs from enhanced precipitation in the ITCZ combined with the shallow ocean mixed layer in this region drive elevated seawater  $\text{Hg}^0$  concentrations. Modeled seawater  $\text{Hg}^0$  concentrations reproduce observed peaks in the ITCZ of both the Atlantic and Pacific Oceans but underestimate its magnitude, likely due to insufficient deep convective scavenging of oxidized Hg from the upper troposphere. Our results demonstrate the importance of scavenging of reactive mercury in the upper atmosphere driving variability in seawater  $\text{Hg}^0$  and net Hg inputs to biologically productive regions of the tropical ocean.



## INTRODUCTION

Air–sea exchange of elemental mercury ( $\text{Hg}^0$ ) plays a critical role in the global mercury (Hg) cycle by extending the lifetime of anthropogenic Hg actively cycling in the environment.<sup>1,2</sup> Most human exposure to methylmercury, a neurotoxin, is from pelagic species such as tuna harvested from the open ocean.<sup>3,4</sup> Reduction of inorganic divalent mercury ( $\text{Hg}^{\text{II}}$ ) in seawater to form  $\text{Hg}^0$  and subsequent evasion to the atmosphere directly reduces the reservoir available for conversion to methylmercury.<sup>5</sup> Limited observational data on atmospheric and aquatic  $\text{Hg}^0$  have hampered our ability to model air–sea exchange on a global scale and predict responses to changes in ocean biogeochemistry.<sup>6,7</sup> Here, we report new high-resolution data from the Pacific Ocean on atmospheric and aquatic  $\text{Hg}^0$  concentrations measured across a wide range of seawater temperature, salinity, and productivity. We use these data to better understand environmental drivers of aqueous  $\text{Hg}^0$  formation and evasion and discuss improvements to modeling capability motivated by these results and a previous study in the Atlantic Ocean.

Regional variability in  $\text{Hg}^0$  evasion mainly reflects differences in turbulent mixing of the surface ocean (wind, bubbles, temperature) and  $\text{Hg}^0$  concentrations in seawater.<sup>8,9</sup> Atmospheric  $\text{Hg}^0$  concentrations in the marine boundary layer are less variable than surface seawater.<sup>6</sup> Atmospheric deposition is the main source of Hg to the open ocean and plays a large role in determining the pool of  $\text{Hg}^{\text{II}}$  available for reduction.<sup>8,10</sup> An additional  $\sim 40\%$  of global Hg inputs to the surface mixed layer of the ocean is from subsurface ocean upwelling, seasonal entrainment, and Ekman pumping.<sup>11,12</sup>

Data on variability in  $\text{Hg}^0$  concentrations in open ocean regions across large gradients in seawater temperature, salinity, productivity, precipitation, and winds are severely limited. Early studies in the Equatorial Pacific suggested that the highest  $\text{Hg}^0$  concentrations and associated evasion occur in productive upwelling regions of the ocean due to enhanced biological

Received: June 26, 2014

Revised: August 26, 2014

Accepted: August 29, 2014

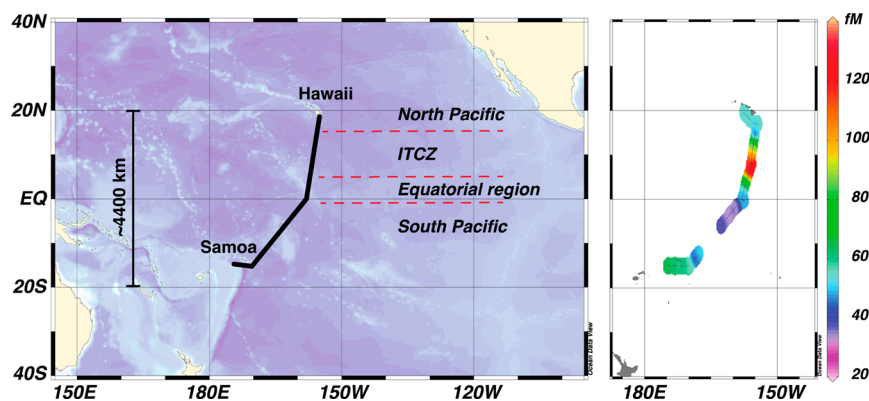


**Figure 1.** Sampling regions and measured seawater  $\text{Hg}^0$  concentrations on the METZYME cruise between October 1 and 24, 2011.

reduction, but spatial coverage of measurements was limited.<sup>5,13</sup> More recent work suggests that photochemical oxidation and reduction of aquatic Hg species occurs much faster than biotic reduction. Elevated ocean productivity may decrease seawater  $\text{Hg}^0$  concentrations through enhanced sorption and scavenging of particle associated  $\text{Hg}^{\text{II}}$  that would otherwise be reduced and evaded.<sup>6,14,15</sup>

Along a latitudinal transect of the Atlantic Ocean, Kuss et al.<sup>16</sup> reported a strong tropical maximum in  $\text{Hg}^0$  concentrations associated with the intertropical convergence zone (ITCZ) and significantly lower values in the equatorial upwelling zone, subtropics, and midlatitudes. The authors attributed this spatial variability to a combination of high precipitation, rapid  $\text{Hg}^{\text{II}}$  photoreduction due to intense solar radiation, and low wind speeds. Recent modeling efforts have not captured this gradient in  $\text{Hg}^0$  concentrations between the ITCZ and adjacent areas<sup>11</sup> and some suggest elevated concentrations in upwelling regions.<sup>12</sup>

Here, we report new high-resolution simultaneous measurements of atmospheric and aquatic  $\text{Hg}^0$  concentrations along a latitudinal transect ( $\sim 20^\circ\text{N}$  to  $\sim 15^\circ\text{S}$ ) of the Pacific Ocean that captures a large gradient in salinity, temperature, meteorology, productivity, and oceanographic circulation. We combine these data with previously published observations from the Atlantic Ocean to better understand latitudinal patterns in seawater  $\text{Hg}^0$  concentrations. We use these observations to evaluate a modeling analysis of Hg inputs and losses to the surface ocean and discuss implications for improving global air–sea exchange estimates.

## MATERIALS AND METHODS

**Field Measurements.** We collected high-resolution (5 min temporal resolution) simultaneous measurements of atmospheric and aquatic gaseous  $\text{Hg}^0$  along the METZYME cruise track in the Pacific Ocean between 1 and 24 October 2011 from  $20^\circ\text{N}$  to  $15^\circ\text{S}$  (Figure 1). Simultaneous aquatic and atmospheric measurements allow for more accurate estimates of air–sea exchange and the high-resolution of measurements collected here allows for a thorough analysis of spatial and temporal variability in concentrations and fluxes.

Atmospheric  $\text{Hg}^0$  was measured using a Tekran 2537A mercury vapor analyzer placed 10 m above the water in front of the ship's bridge. The instrument was calibrated daily using the internal calibration source and had a detection limit of  $<0.2 \text{ ng m}^{-3}$ . For aqueous  $\text{Hg}^0$ , we collected seawater from the ship's intake placed at 7 m depth at the front of the ship. We measured seawater  $\text{Hg}^0$  concentrations using the automatic

continuous equilibrium system described in detail in Andersson et al.<sup>17</sup> Briefly, aqueous  $\text{Hg}^0$  is sparged into the headspace of the sampler allowing concentrations to be calculated from the atmospheric measurement and Henry's law constant. The Tekran 2537B used during water sampling was calibrated daily using the internal calibration source and the detection limit was  $<2 \text{ fM}$  for seawater  $\text{Hg}^0$ . Prior studies compared aqueous  $\text{Hg}^0$  concentrations measured using the continuous sampler to those with manual methods and verified consistency over a range of seawater temperatures.<sup>6,9,17</sup> Performance of the continuous sampler has also been verified in the laboratory prior to cruises on multiple occasions by injection and recovery of external standards.<sup>6,9</sup>

We aggregated all measurements including standard underway measurements of wind speed, salinity, water temperature, and in situ fluorescence (a proxy for algal productivity) into 1 h averages for statistical analyses.<sup>18</sup> Averaging over an hour is reasonable as the short-term variability in the measurements was small (typical variability is 3% and 10% for 1 h observations of  $\text{Hg}^0$  in air and water, respectively;  $n = 12$  5-min samples per hour). Dissolved gaseous Hg in surface seawater is assumed to be mainly  $\text{Hg}^0$  because many studies have shown that surface seawater ( $<50 \text{ m}$  depth) generally contains  $<5\%$  dimethylmercury.<sup>19–21</sup>

**Modeling.** Measured aquatic and atmospheric  $\text{Hg}^0$  concentrations were used to estimate air–sea fluxes. We used the Nightingale et al.<sup>22</sup> parameterization for instantaneous wind speeds, the Henry's law coefficient for  $\text{Hg}^0$ ,<sup>23</sup> a temperature-corrected Schmidt number for  $\text{CO}_2$ ,<sup>24</sup> and the Wilke–Chang method for estimating temperature- and salinity-corrected  $\text{Hg}^0$  diffusivity.<sup>25</sup> Several values have been proposed for the diffusivity of  $\text{Hg}^0$ , as discussed by Kuss et al.,<sup>26</sup> and variability in this parameter is included in Supporting Information Table S1.<sup>27</sup> We selected the Nightingale et al.<sup>22</sup> parameterization because it provides a midrange estimate of air–sea exchange.<sup>28,29</sup>

We compare observed seawater  $\text{Hg}^0$  concentrations to modeling simulations for Hg species in the ocean from the MIT General Circulation Model (MITgcm) forced by the atmospheric simulation in the GEOS-Chem chemical transport model (CTM).<sup>30</sup> The MITgcm includes both lateral and vertical transport of Hg species due to ocean circulation and settling of suspended particles.<sup>30,35</sup> The ocean simulation is driven by Hg deposition inputs from the GEOS-Chem atmospheric model (version v9-01-02) using 2006–2009 meteorological data (GEOS-5), as described in Zhang et al.<sup>31</sup> It has a horizontal resolution of  $1^\circ \times 1^\circ$  and 23 vertical levels.<sup>32</sup>

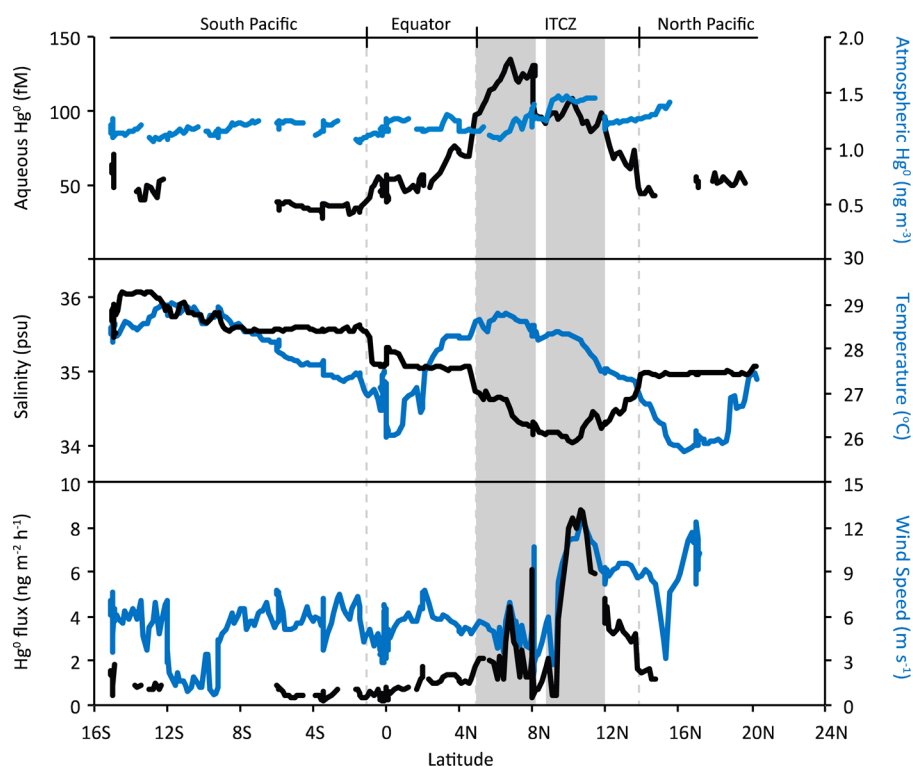


**Figure 2.** Latitudinal variability in measured atmospheric and seawater  $\text{Hg}^0$  concentrations, associated evasion, and environmental properties on the METZYME cruise. Shaded areas denote statistically different regions for  $\text{Hg}^0$  concentrations within the region reflecting the ITCZ.

**Table 1. Summary of Observations Across Oceanographic Regimes of the Pacific Ocean<sup>a</sup>**

	North Pacific 14–20°N	ITCZ 5–14°N	Equator 1°S–5°N	South Pacific 1–15°S
$\text{Hg}_{\text{atm}}^0$ ( $\text{ng m}^{-3}$ )	$1.32 \pm 0.05$	$1.27 \pm 0.10$	$1.18 \pm 0.05$	$1.15 \pm 0.05$
$\text{Hg}_{\text{aq}}^0$ (fm)	$51.3 \pm 4.1$	$104.7 \pm 19.9$	$53.0 \pm 10.3$	$47.0 \pm 13.3$
$\text{Hg}^0$ flux ( $\text{ng m}^{-2} \text{h}^{-1}$ )	$1.4 \pm 0.2$	$3.2 \pm 2.2$	$0.7 \pm 0.4$	$0.8 \pm 0.4$
wind speed ( $\text{m s}^{-1}$ )	$9.8 \pm 2.5$	$6.6 \pm 2.9$	$5.1 \pm 1.2$	$5.6 \pm 1.7$
sea surface temperature ( $^{\circ}\text{C}$ )	$26.1 \pm 0.35$	$28.2 \pm 0.39$	$26.9 \pm 0.70$	$28.3 \pm 0.51$
salinity (psu)	$35.0 \pm 0.02$	$34.3 \pm 0.15$	$35.1 \pm 0.11$	$35.7 \pm 0.17$
fluorescence (unitless) <sup>b</sup>	$99.7 \pm 2.6$	$116.3 \pm 23.6$	$209.3 \pm 50.7$	$139.3 \pm 42.3$
Chla ( $\text{mg m}^{-3}$ )	0.03–0.06	0.06–0.09	0.12–0.27	0.06–0.15
mixed layer depth (m)	50	30	100	150

<sup>a</sup>All regions are significantly different from each other using a Tukey–Kramer test for multiple comparisons except: North Pacific–ITCZ ( $\text{Hg}_{\text{atm}}^0$ ); North Pacific–Equator ( $\text{Hg}_{\text{aq}}^0$ ); North Pacific–South Pacific ( $\text{Hg}_{\text{aq}}^0$ ); Equator–South Pacific ( $\text{Hg}^0$  flux and wind speed); ITCZ–South Pacific (sea surface temperature). <sup>b</sup>Fluorescence was measured with a baseline  $\sim 95$  and provides a relative indicator of variability in productivity across the cruise track but cannot be compared between cruises because the baseline value is cruise specific.

and includes an ecological simulation of carbon and plankton dynamics (the Darwin model). Organic carbon dynamics are important for parameterizing vertical Hg transport and the available pool of  $\text{Hg}^{\text{II}}$  for reduction.<sup>33</sup> Physical advection and diffusion of tracers are driven by ocean circulation data from ECCO-GODAE state estimates.<sup>34</sup> Differences attributable to variability in meteorological years of the observations are expected to be small. For example, interannual variability in wet deposition between 2006 and 2011 was  $<5\%$  for the Pacific (160°N transect) and the Atlantic (25°W transect). Rate coefficients for photochemical and biologically driven redox reactions between  $\text{Hg}^0$  and  $\text{Hg}^{\text{II}}$ , sorption to suspended particles, and parameterization of air–sea exchange estimates are from published and previously evaluated models of Hg fate in the ocean.<sup>11,35</sup> The ocean model was run with repeated circulation and external forcing from current day rivers and

deposition for 10 years.<sup>36</sup> We use this analysis to gain insights into Hg inputs and losses in the surface ocean mixed layer.

## RESULTS AND DISCUSSION

We grouped observations across the METZYME cruise track into four regions representing: (1) the North Pacific (14–20°N), (2) the ITCZ (5–14°N), (3) the Equatorial Pacific (5°N–1°S), and (4) the South Pacific (1–15°S) (Figure 1 and Supporting Information Figure S1). These are specified based on differences in ocean circulation and atmospheric processes that vary seasonally and result in measurable differences in seawater temperature, salinity, and fluorescence<sup>37</sup> (Figure 2 and Table 1). In the North Pacific, seawater is cold with characteristically low productivity. Approaching the ITCZ, seawater temperature increases and salinity declines as the result of high precipitation rates. Surface waters in the ITCZ are subject to substantial wind driven Ekman pumping and are

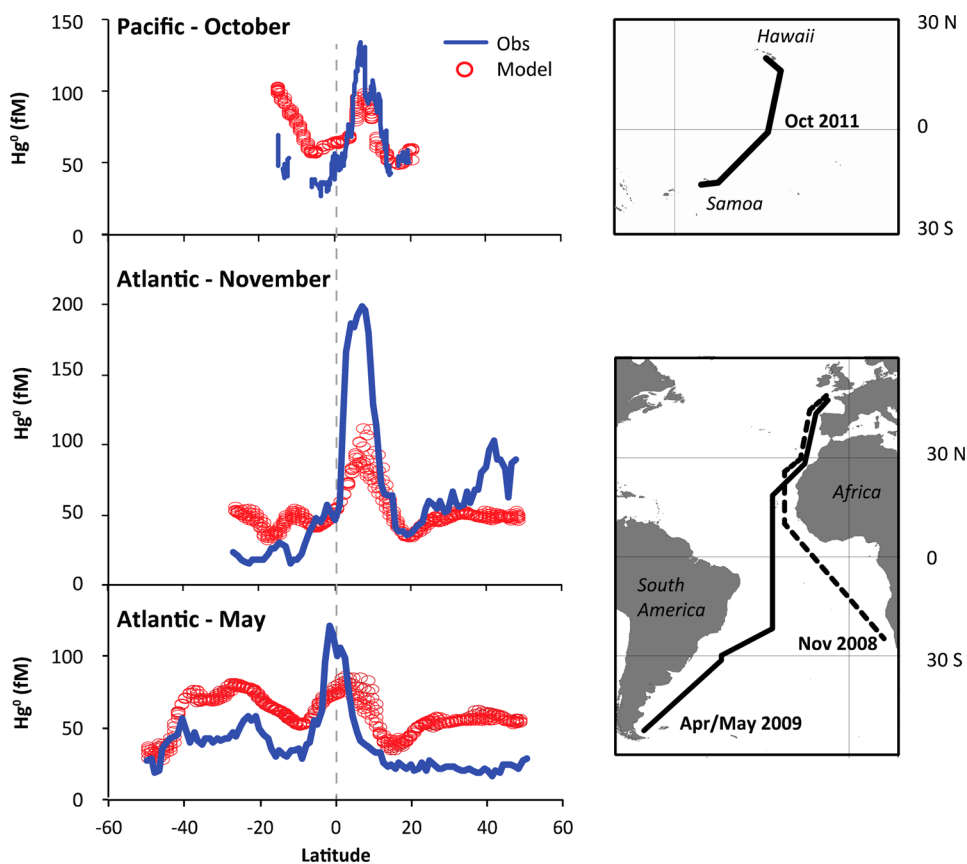


**Figure 3.** Comparison of modeled (red) and observed (blue) latitudinal gradients in  $\text{Hg}^0$  along cruise tracks in the Pacific and the Atlantic Oceans. Model results are from an ocean general circulation model (MITgcm) based on the Hg simulation developed by Zhang et al.<sup>30</sup> within  $\pm 2$  degrees of the cruise track with atmospheric inputs from the GEOS-Chem global Hg model.<sup>31</sup> Data from the Atlantic Ocean are from Kuss et al.<sup>16</sup>

stratified. The equatorial region is dominated by the low temperatures of the South Equatorial Current and high productivity due to upwelling nutrients, whereas the South Pacific has warmer high salinity water with intermediate productivity.<sup>38,39</sup>

**Latitudinal Variability in  $\text{Hg}^0$ .** Table 1 and Figure 2 show measured atmospheric and aquatic  $\text{Hg}^0$  concentrations along the cruise track, associated evasion fluxes, and ancillary data. Atmospheric  $\text{Hg}^0$  concentrations are significantly elevated in the North Pacific ( $14\text{--}20^\circ\text{N}$ ) and ITCZ ( $5\text{--}14^\circ\text{N}$ ) compared to the equatorial ( $1\text{--}5^\circ\text{N}$ ) and South Pacific ( $1\text{--}15^\circ\text{S}$ ) (Tukey–Kramer test,  $p < 0.001$ ). Mean concentrations ranged from  $1.15 \text{ ng m}^{-3}$  in the South Pacific up to  $1.32 \text{ ng m}^{-3}$  in the North Pacific (Table 1). This pattern is consistent with enrichment of atmospheric mercury in the northern hemisphere from anthropogenic sources.<sup>40,41</sup>

Early studies suggested enhanced seawater  $\text{Hg}^0$  concentrations in equatorial upwelling regions.<sup>13</sup> Data with much higher spatial and temporal resolution collected here show relatively low concentrations of atmospheric  $\text{Hg}^0$  (mean  $1.18 \text{ ng m}^{-3}$ ) and aquatic  $\text{Hg}^0$  (mean  $53 \text{ fM}$ ) in the equatorial region ( $1\text{--}5^\circ\text{N}$ ) compared to more northern areas.  $\text{Hg}^{\text{II}}$  in seawater has a strong affinity for organic particles and is rapidly removed from the mixed layer during carbon export.<sup>11</sup> Indicators of ocean productivity and associated abundance of biological particles include chlorophyll a (Chla) and fluorescence. High Chla and fluorescence in the equatorial region (Table 1), supports the premise that enhanced removal of  $\text{Hg}^{\text{II}}$  associated with suspended particles is likely occurring, lowering the  $\text{Hg}^{\text{II}}$

pool available for reduction and  $\text{Hg}^0$  concentrations in the equatorial upwelling region.

Seawater  $\text{Hg}^0$  concentrations differ by almost a factor of 3 across regions compared to  $<20\%$  variability in atmospheric  $\text{Hg}^0$  concentrations. Seawater  $\text{Hg}^0$  concentrations were highest in the warm, low salinity waters of the ITCZ ( $\sim 130 \text{ fM}$ ) and remained low and fairly stable outside this region ( $\sim 47\text{--}53 \text{ fM}$ ). This variability is much higher than observed in our previous work near Bermuda where the average concentration varied by less than a factor of 2 across four cruises over two years.<sup>6</sup> We attribute high seawater  $\text{Hg}^0$  concentrations reported here in the ITCZ region to rapid reduction of high Hg inputs through wet deposition. The shallow mixed layer observed during sampling makes the impact of these enhanced inputs more pronounced (Table 1).

We did not measure total Hg concentrations in precipitation on the cruise but previously reported total Hg concentrations in wet deposition from across the Pacific ( $14\text{--}75 \text{ pM}$ )<sup>41–43</sup> are  $\sim 50$  times higher than seawater concentrations. Seawater  $\text{Hg}^0$  and salinity were strongly anticorrelated ( $R^2 = 0.63$ ,  $p < 0.01$ ) across the cruise. Precipitation rates in the ITCZ ( $2.5\text{--}3.0 \text{ m yr}^{-1}$ ) are much higher than adjacent areas ( $0.3\text{--}1.0 \text{ m yr}^{-1}$ ) (Supporting Information Figure S2).<sup>44</sup> Deep convective precipitation scavenges upper tropospheric air enriched in  $\text{Hg}^{\text{II}}$ , resulting in high rainwater concentrations.<sup>45</sup> A study from the Western Pacific region with deep convection reports an average summertime concentration of total Hg in wet deposition of  $\sim 58 \text{ pM}$ .<sup>46</sup>

Seawater  $\text{Hg}^0$  also varied significantly within the ITCZ ( $t$  test,  $p < 0.001$ ). Concentrations increased south of  $8^\circ\text{N}$  (shaded area to the left in Figure 2) due to a combination of higher inputs from precipitation and significantly lower wind speeds ( $t$  test,  $p < 0.001$ ). Satellite data show an average rainfall of  $1\text{--}3\text{ mm h}^{-1}$  during the cruise in the southern part of the ITCZ and little precipitation in the northern part<sup>47</sup> (Supporting Information Figure S2). The presence of a vertical salinity gradient in the mixed layer in the southern ITCZ but not the northern part supports this premise (Supporting Information Figure S3) and indicates that the ITCZ is moving south. Precipitation of  $2\text{ mm h}^{-1}$  with  $50\text{ pM Hg}$  over just 1 day ( $48\text{ mm d}^{-1}$ ) would increase seawater  $\text{Hg}$  concentration within the upper 10 m by  $\sim 25\%$ , assuming a background concentration of  $\sim 1\text{ pM}$ .<sup>48</sup> Sustained precipitation over several days could therefore explain the observed increase in concentrations in the southern ITCZ mixed layer ( $\sim 30\text{ m}$ ) even if washout of tropospheric  $\text{Hg}^{\text{II}}$  reduced concentrations in precipitation.

Atmospheric  $\text{Hg}^0$  is elevated in the northern part of the ITCZ temporarily influenced by the Northeastern trade winds, likely due to the highest evasion fluxes of the cruise observed in this region ( $>8\text{ ng m}^{-2}\text{ h}^{-1}$ ). Lower seawater  $\text{Hg}^0$  is also apparent in the northern ITCZ compared to southern regions, but the observed gradient in concentrations is likely attributable to differences in inputs (wet deposition) rather than losses as discussed above. The rapid equilibrium established between  $\text{Hg}^{\text{II}}$  and  $\text{Hg}^0$  in surface waters<sup>14</sup> means that changes in  $\text{Hg}^0$  concentrations reflect variability in the larger pool of inorganic  $\text{Hg}$  species. The relative increase in evasion in the northern ITCZ is, thus, not large enough to explain the observed north–south ITCZ gradient in seawater  $\text{Hg}^0$ .

**Latitudinal Variability in Evasion.** Net air–sea exchange in the ITCZ (maximum:  $8.7\text{ ng m}^{-2}\text{ h}^{-1}$ ) was more than 4-fold greater (mean:  $3.2 \pm 2.2\text{ ng m}^{-2}\text{ h}^{-1}$ ) than in the more southerly regions ( $0.7\text{--}0.8\text{ ng m}^{-2}\text{ h}^{-1}$ ) and more than 2-fold greater than in the North Pacific (Table 1). These differences are due to a combination of high seawater  $\text{Hg}^0$  and the North Eastern trade winds temporarily overlapping with the northern part of the ITCZ during our cruise (Figure 2). Wind speeds throughout the cruise were lowest between  $8$  and  $12^\circ\text{S}$  ( $<3\text{ m s}^{-1}$ ), fairly stable between  $8^\circ\text{S}$ – $4^\circ\text{N}$ , dipped below  $3\text{ m s}^{-1}$  again in the southern part of the ITCZ and then rapidly increased to  $12\text{ m s}^{-1}$  in the northern regions (Figure 2). Although highest overall  $\text{Hg}^0$  concentrations occurred in the southern part of the ITCZ, the highest evasion fluxes were located in the northern region at the intersection of high wind speeds (associated with movement of ITCZ south) and elevated seawater  $\text{Hg}^0$  concentrations. Low seawater  $\text{Hg}^0$  concentrations in the North Pacific between  $12$  and  $15^\circ\text{N}$  resulted in lower evasion despite high wind speeds. These observations reinforce the importance of understanding variability in seawater  $\text{Hg}^0$  as a control on the magnitude of air–sea exchange, a factor that has been neglected in some broad scale studies.<sup>49</sup>

**Large Scale Drivers of  $\text{Hg}^0$  Across Ocean Basins.** Similar latitudinal variability in seawater  $\text{Hg}^0$  is seen when comparing data from the Pacific Ocean reported here to data from the Atlantic Ocean<sup>16</sup> (Figure 3). Kuss et al.<sup>16</sup> also observed elevated  $\text{Hg}^0$  concentrations in the low salinity, warm waters of the Equatorial Atlantic Ocean across two seasons. Peak seawater  $\text{Hg}^0$  in the Atlantic Ocean tracked the movement of the ITCZ between sampling periods in November and May (Figure 3). High  $\text{Hg}^0$  concentrations in the ITCZ in the

Atlantic springtime ( $\sim 130\text{ fM}$ ) were similar to those reported here for the Pacific ( $\sim 130\text{ fM}$ ), whereas concentrations measured during the Atlantic fall were higher ( $\sim 220\text{ fM}$ ).  $\text{Hg}^0$  concentrations in the tropical Atlantic ( $15^\circ\text{S}$ – $15^\circ\text{N}$ ) ranged between  $35$  and  $60\text{ fM}$  and also matched our observations in the Pacific ( $\sim 50\text{ fM}$ ). Variability in evasion fluxes was similar for the Atlantic and Pacific ranging  $\sim 4$  fold across regions with highest fluxes where high wind speeds and elevated  $\text{Hg}^0$  coincide in the tropical and subtropical oceans.

Figure 3 compares simulated  $\text{Hg}^0$  in surface seawater ( $0\text{--}10\text{ m}$  depth) using an ocean general circulation model for  $\text{Hg}$  species (MITgcm) forced by the GEOS-Chem atmospheric model to observations from all three cruises. The ocean model reproduces much of the observed latitudinal variability in aqueous  $\text{Hg}^0$  (Figure 3). The model reasonably matches most concentrations outside the ITCZ (observations:  $40 \pm 18\text{ fM}$ , model:  $54 \pm 14\text{ fM}$ ) but only captures on average 60% of the amplitude of the peak in the ITCZ (range  $45\text{--}70\%$  across cruises; observations:  $124 \pm 41\text{ fM}$ , model:  $74 \pm 9\text{ fM}$ ). Kuss et al.<sup>16</sup> suggested that a combination of a shallow mixed layer and high solar radiation could cause the elevated  $\text{Hg}^0$  concentrations in the ITCZ, but these processes are accounted for in our model simulation.<sup>11,30</sup>

Concentrations of  $\text{Hg}^0$  in the surface ocean reflect the overall pool of inorganic  $\text{Hg}$  because there is a rapid equilibrium established between  $\text{Hg}^0$  and  $\text{Hg}^{\text{II}}$  in seawater, as discussed above.<sup>14</sup> Figure 4 shows the relative importance of various input and loss pathways for inorganic  $\text{Hg}$  in the surface ocean of the cruise regions sampled. Net inputs from atmospheric deposition are the predominant source in the ITCZ across the Atlantic and Pacific regions. A sensitivity simulation shows that modeled seawater  $\text{Hg}^0$  is almost proportionally affected by changes in atmospheric  $\text{Hg}^{\text{II}}$  inputs in the ITCZ (20% change in deposition resulted in  $14\text{--}16\%$  change in  $\text{Hg}^0$  in the ITCZ and  $6\text{--}16\%$  elsewhere; Supporting Information Figure S4). Thus, low bias in modeled seawater  $\text{Hg}^0$  in the ITCZ compared to observations likely reflects insufficient  $\text{Hg}$  deposition in the atmospheric simulation (GEOS-Chem) for this region.

The GEOS-Chem model reproduces precipitation in the ITCZ fairly well compared to satellite observations,<sup>47</sup> suggesting the model underestimation is related to limited supply of  $\text{Hg}^{\text{II}}$  in precipitation. Deep convective cloud systems and high precipitation loads distinguish the ITCZ from other parts of the tropical ocean,<sup>44,50</sup> and recent work has shown that cumulonimbus clouds reaching altitudes of  $10\text{--}14\text{ km}$  may enhance  $\text{Hg}^{\text{II}}$  scavenging compared to stratiform clouds ( $\sim 4\text{ km}$ ) for the same precipitation load.<sup>51</sup> Insufficient deposition in areas of deep convection has also been noted in comparisons of GEOS-Chem simulated deposition to measured  $\text{Hg}$  wet deposition from the MDN network data at mid latitudes.<sup>31,52</sup> In both the midlatitudes and the tropics, this discrepancy could be caused by high concentrations of  $\text{Hg}^{\text{II}}$  in the upper troposphere suggested by recent observations<sup>53</sup> that are not captured in the GEOS-Chem model. Alternately, the GEOS-Chem model may underestimate the frequency of precipitation events in the upper troposphere<sup>54</sup> negatively affecting the wet scavenging of contaminants. As evidence for the latter, Wang et al.<sup>54</sup> found that GEOS-Chem greatly overestimates upper tropospheric black carbon concentrations in the tropics. Our work suggests the need for additional measurements of wet deposition in tropical areas and improved understanding of atmospheric  $\text{Hg}$  dynamics in regions with deep convection to

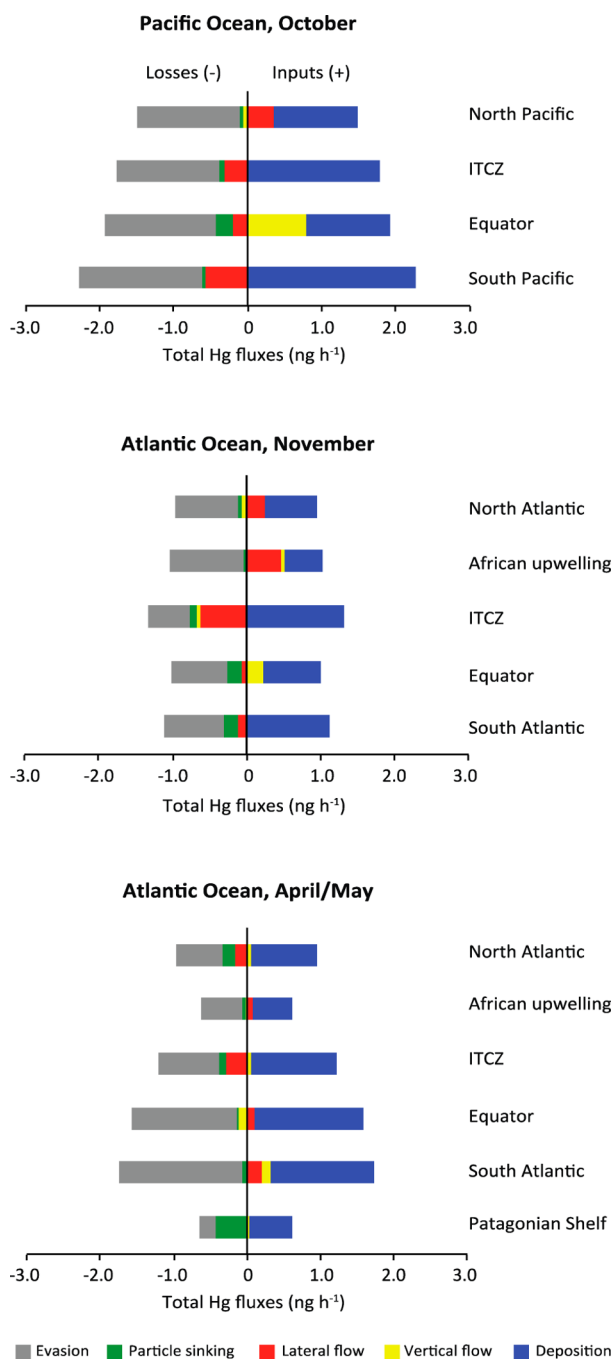


**Figure 4.** Modeled inputs and losses of Hg in the ocean mixed layer across the cruise regions sampled. Results are presented as monthly averages from an ocean general circulation model (MITgcm) Hg simulation.<sup>30</sup> Model comparison with observations indicates a low bias in atmospheric inputs in the ITCZ (Figure 3). The water column budget for the surface ocean mixed layer is based on regional averages for inputs and losses to the surface ocean (a 1 m<sup>2</sup> surface area and 55 m deep water column) along each cruise track from the model.

better quantify mercury deposition and resulting seawater concentrations in the tropics.<sup>55</sup>

Figure 4 illustrates the importance of lateral seawater flow in the surface ocean for redistributing enhanced atmospheric mercury deposited in the ITCZ region. Lateral transport of Hg is clearly important for a variety of ocean regions<sup>30,35</sup> and has not been captured in earlier GEOS-Chem simulations of air–sea exchange.<sup>11,56,57</sup> Ekman pumping is particularly pronounced

in the ITCZ region, resulting in strong horizontal outflow of Hg in the surface ocean to other regions of the tropical ocean. Upwelling in the equatorial region and along the African coast reintroduces Hg from the subsurface ocean into the surface ocean.<sup>58,59</sup> In highly productive regions such as the Patagonian Shelf in the Atlantic, losses from particle settling can exceed evasion, and will vary seasonally. These results clearly illustrate the importance of adequately capturing both Hg redox chemistry and physical transport processes, including seasonality, in the atmosphere and ocean to resolve air–sea exchange estimates. Results presented here suggest enhanced net atmospheric Hg inputs in the ITCZ are redistributed through lateral ocean transport of surface waters (Figure 4) to biologically productive regions of the tropical ocean.

## ■ ASSOCIATED CONTENT

### § Supporting Information

Additional information, includes all data for atmospheric and aquatic Hg<sup>0</sup> from the Atlantic and Pacific Oceans and associated evasion fluxes. This material is available free of charge via the Internet at <http://pubs.acs.org>.

## ■ AUTHOR INFORMATION

### Corresponding Author

\*E-mail: [alsoeren@hsph.harvard.edu](mailto:alsoeren@hsph.harvard.edu)

### Notes

The authors declare no competing financial interest.

## ■ ACKNOWLEDGMENTS

We acknowledge financial support from the U.S. National Science Foundation, Chemical Oceanography division (NSF OCE-1130549). A.L.S. acknowledges financial support from the Carlsberg Foundation. We thank the captain, science technicians, and crew of the *RV Kilo Moana*, and Chief Scientists Carl Lamborg and Mak Saito (WHOI). We thank Elizabeth S. Corbitt, Helen Amos, and Johan Schmidt for helpful discussions.

## ■ REFERENCES

- (1) Corbitt, E. S.; Jacob, D. J.; Holmes, C. D.; Streets, D. G.; Sunderland, E. M. Global Source-Receptor Relationships for Mercury Under Present-Day and 2050 Emissions Scenarios. *Environ. Sci. Technol.* **2011**, *45* (24), 10477–10484.
- (2) Amos, H. M.; Jacob, D. J.; Streets, D. G.; Sunderland, E. M. Legacy Impacts of All-Time Anthropogenic Emissions on the Global Mercury Cycle. *Biogeochem. Cycles* **2013**, *27*, 1–12.
- (3) Sunderland, E. M. Mercury Exposure from Domestic and Imported Estuarine and Marine Fish in the US Seafood Market. *Environ. Health Perspect.* **2007**, *115* (2), 235–242.
- (4) Mahaffey, K. R.; Sunderland, E. M.; Chan, H. M.; Choi, A. L.; Grandjean, P.; Marien, K.; Oken, E.; Sakamoto, M.; Schoeny, R.; Weihe, P.; Yan, C. H.; Yasutake, A. Balancing the Benefits of N-3 Polyunsaturated Fatty Acids and the Risks of Methylmercury Exposure from Fish Consumption. *Nutr. Rev.* **2011**, *69* (9), 493–508.
- (5) Mason, R. P.; Fitzgerald, W. F. The Distribution and Biogeochemical Cycling of Mercury in the Equatorial Pacific-Ocean. *Deep-Sea Res., Part I* **1993**, *40* (9), 1897–1924.
- (6) Soerensen, A. L.; Mason, R. P.; Balcom, P. H.; Sunderland, E. M. Drivers of Surface Ocean Mercury Concentrations and Air–Sea Exchange in the West Atlantic Ocean. *Environ. Sci. Technol.* **2013**, *47*, 7757–7765.
- (7) Doney, S. C. The Growing Human Footprint on Coastal and Open-Ocean Biogeochemistry. *Science* **2010**, *328* (5985), 1512–1516.
- (8) Mason, R. P.; Sheu, G. R. Role of the Ocean in the Global Mercury Cycle. *Global Biogeochem. Cycles* **2002**, *16*, (4).

- (9) Andersson, M. E.; Sommar, J.; Gardfeldt, K.; Lindqvist, O. Enhanced Concentrations of Dissolved Gaseous Mercury in the Surface Waters of the Arctic Ocean. *Mar. Chem.* **2008**, *110* (3–4), 190–194.
- (10) Sunderland, E. M.; Mason, R. P. Human Impacts on Open Ocean Mercury Concentrations. *Global Biogeochem. Cycles* **2007**, *21* (4), Artn Gb4022.
- (11) Soerensen, A. L.; Sunderland, E. M.; Holmes, C. D.; Jacob, D. J.; Yantosca, R. M.; Skov, H.; Christensen, J. H.; Strode, S. A.; Mason, R. P. An Improved Global Model for Air–sea Exchange of Mercury: High Concentrations over the North Atlantic. *Environ. Sci. Technol.* **2010**, *44* (22), 8574–8580.
- (12) Strode, S. A.; Jaegle, L.; Selin, N. E.; Jacob, D. J.; Park, R. J.; Yantosca, R. M.; Mason, R. P.; Slemr, F. Air–sea Exchange in the Global Mercury Cycle. *Global Biogeochem. Cycles* **2007**, *21*, (1).
- (13) Fitzgerald, W. F.; Gill, G. A.; Kim, J. P. An Equatorial Pacific–Ocean Source of Atmospheric Mercury. *Science* **1984**, *224* (4649), 597–599.
- (14) Qureshi, A.; O’Driscoll, N. J.; MacLeod, M.; Neuhold, Y. M.; Hungerbuhler, K. Photoreactions of Mercury in Surface Ocean Water: Gross Reaction Kinetics and Possible Pathways. *Environ. Sci. Technol.* **2010**, *44* (2), 644–649.
- (15) O’Driscoll, N. J.; Siciliano, S. D.; Lean, D. R. S.; Amyot, M. Gross Photoreduction Kinetics of Mercury in Temperate Freshwater Lakes and Rivers: Application to a General Model of Dgm Dynamics. *Environ. Sci. Technol.* **2006**, *40* (3), 837–843.
- (16) Kuss, J.; Züllicke, C.; Pohl, C.; Schneider, B. Atlantic Mercury Emission Determined from Continuous Analysis of the Elemental Mercury Sea–Air Concentration Difference within Transects between 50 Degrees N and 50 Degrees S. *Global Biogeochem. Cycles* **2011**, *25*.
- (17) Andersson, M. E.; Gardfeldt, K.; Wangberg, I. A Description of an Automatic Continuous Equilibrium System for the Measurement of Dissolved Gaseous Mercury. *Anal. Bioanal. Chem.* **2008**, *391* (6), 2277–2282.
- (18) SOEST, University of Hawaii (<http://www.soest.hawaii.edu>): *Formats of Logged Data: Updated 23-Jul-10* Ftp site: <ftp://ftp.soest.hawaii.edu/> (Access date: August 2014).
- (19) Horvat, M.; Kotnik, J.; Logar, M.; Fajon, V.; Zvonaric, T.; Pirrone, N. Speciation of Mercury in Surface and Deep–Sea Waters in the Mediterranean Sea. *Atmos. Environ.* **2003**, *37*, S93–S108.
- (20) Bowman, K. L.; Hammerschmidt, C. R.; Lamborg, C. H.; Swarr, G. Mercury in the North Atlantic Ocean: The U.S. Geotraces Zonal and Meridional Sections. *Deep-Sea Res., Part II* **2014**, DOI: 10.1016/j.dsr2.2014.07.004.
- (21) Hammerschmidt, C. R.; Bowman, K. L. Vertical Methylmercury Distribution in the Subtropical North Pacific Ocean. *Mar. Chem.* **2012**, *132*, 77–82.
- (22) Nightingale, P. D.; Malin, G.; Law, C. S.; Watson, A. J.; Liss, P. S.; Liddicoat, M. I.; Boutin, J.; Upstill-Goddard, R. C. In Situ Evaluation of Air–sea Gas Exchange Parameterizations Using Novel Conservative and Volatile Tracers. *Global Biogeochem. Cycles* **2000**, *14* (1), 373–387.
- (23) Andersson, M. E.; Gardfeldt, K.; Wangberg, I.; Stromberg, D. Determination of Henry’s Law Constant for Elemental Mercury. *Chemosphere* **2008**, *73* (4), 587–592.
- (24) Poissant, L.; Amyot, M.; Pilote, M.; Lean, D. Mercury Water–Air Exchange over the Upper St. Lawrence River and Lake Ontario. *Environ. Sci. Technol.* **2000**, *34* (15), 3069–3078.
- (25) Wilke, C. R.; Chang, P. Correlation of Diffusion Coefficients in Dilute Solutions. *AIChE J.* **1955**, *1* (2), 264–270.
- (26) Kuss, J.; Holzmann, J.; Ludwig, R. An Elemental Mercury Diffusion Coefficient for Natural Waters Determined by Molecular Dynamics Simulation. *Environ. Sci. Technol.* **2009**, *43* (9), 3183–3186.
- (27) Kuss, J. Water–Air Gas Exchange of Elemental Mercury: An Experimentally Determined Mercury Diffusion Coefficient for Hg<sub>0</sub> Water–Air Flux Calculations. *Limnol. Oceanogr.* **2014**, *59* (5), 1461–1467.
- (28) Wanninkhof, R. Relationship between Wind-Speed and Gas-Exchange over the Ocean. *J. Geophys. Res. Oceans* **1992**, *97* (C5), 7373–7382.
- (29) Liss, P. S.; Merlivat, L. Air–sea Exchange Rates: Introduction and Synthesis. In *The Role of Air–Sea Exchange in Geochemical Cycling*; Buat-Menard, P., Ed. Reidel Publishing Company: Dordrecht, Netherlands, 1986; pp 113–127.
- (30) Zhang, Y.; Jacob, D. J.; Amos, H. M.; Dutkiewicz, S.; Sunderland, C. J. The role of ocean biogeochemistry and particle dynamics for the fate and transport of river derived mercury. 2014; in preparation.
- (31) Zhang, Y.; Jaegle, L.; van Donkelaar, A.; Martin, R. V.; Holmes, C. D.; Amos, H. M.; Wang, Q.; Talbot, R.; Artz, R.; Brooks, S.; Luke, W.; Holsen, T. M.; Felton, D.; Miller, E. K.; Perry, K. D.; Schmeltz, D.; Steffen, A.; Tordon, R.; Weiss-Penzias, P.; Zsolway, R. Nested-Grid Simulation of Mercury over North America. *Atmos. Chem. Phys.* **2012**, *12* (14), 6095–6111.
- (32) Marshall, J.; Hill, C.; Perelman, L.; Adcroft, A. Hydrostatic, Quasi-Hydrostatic, and Nonhydrostatic Ocean Modeling. *J. Geophys. Res. Oceans* **1997**, *102* (C3), 5733–5752.
- (33) Dutkiewicz, S.; Follows, M. J.; Bragg, J. G. Modeling the Coupling of Ocean Ecology and Biogeochemistry. *Global Biogeochem. Cycles* **2009**, *23*.
- (34) Wunsch, C.; Heimbach, P. Practical Global Oceanic State Estimation. *Phys. D (Amsterdam, Neth.)* **2007**, *230* (1–2), 197–208.
- (35) Zhang, Y.; Jaegle, L.; Thompson, L. Natural Biogeochemical Cycle of Mercury in a Global Three-Dimensional Ocean Tracer Model. *Global Biogeochem. Cycles* **2014**, *28* (5), 553–570.
- (36) Amos, H. M.; Jacob, D. J.; Kochman, D.; Horowitz, H. M.; Zhang, Y.; Dutkiewicz, S.; Horvat, M.; Corbitt, E. S.; Sunderland, E. M. Global Biogeochemical Implications of Mercury Discharges from Rivers and Sediment Burial. *Environ. Sci. Technol.* **2014**, *48* (16), 9514–9522.
- (37) Reygondeau, G.; Lonhurst, A.; Martinez, E.; Beaugrand, G.; Antoine, D.; Maury, O. Dynamic Biogeochemical Provinces in the Global Ocean. *Global Biogeochem. Cycles* **2013**, *27* (1–13), 1–13.
- (38) Pennington, J. T.; Mahoney, K. L.; Kuwahara, V. S.; Kolber, D. D.; Calienes, R.; Chavez, F. P. Primary Production in the Eastern Tropical Pacific: A Review. *Prog. Oceanogr.* **2006**, *69* (2–4), 285–317.
- (39) Pickard, G. L.; Emery, W. J. *Descriptive Physical Oceanography*, 5th ed.; Pergamon Press: Oxford, U. K., 1990.
- (40) Slemr, F. Trends in Atmospheric Mercury Concentrations over the Atlantic Ocean and at the Wank Summit, and the Resulting Constraints on the Budget of Atmospheric Mercury. In *Global and Regional Mercury Cycles: Sources, Fluxes and Mass Balances*; Baeyens, W., Ed. Kluwer Academic Publishers: Netherlands, 1996; Vol. 21, pp 33–84.
- (41) Fitzgerald, W. F. Cycling of Mercury between the Atmosphere and Oceans. In *The Role of Air–sea Exchange in Geochemical Cycling*; Buat-Menard, P., Ed. D. Reidel Publishing Company: Dordrecht, Netherlands, 1986; Vol. 185, pp 363–408.
- (42) Mason, R. P.; Fitzgerald, W. F.; Vandal, G. M. The Sources and Composition of Mercury in Pacific–Ocean Rain. *J. Atmos. Chem.* **1992**, *14* (1–4), 489–500.
- (43) Laurier, F. J. G.; Mason, R. P.; Whalin, L.; Kato, S. Reactive Gaseous Mercury Formation in the North Pacific Ocean’s Marine Boundary Layer: A Potential Role of Halogen Chemistry. *J. Geophys. Res.-Atmos.* **2003**, *108*, (D17).
- (44) NASA, Tropical Rainfall Measuring Mission (Trmm) Website. <http://pmm.nasa.gov/TRMM/TRMM-based-climatology> (Access date: June 2014).
- (45) Selin, N. E.; Jacob, D. J. Seasonal and Spatial Patterns of Mercury Wet Deposition in the United States: Constraints on the Contribution from North American Anthropogenic Sources. *Atmos. Environ.* **2008**, *42* (21), 5193–5204.
- (46) Sheu, G. R.; Lin, N. H. Characterizations of Wet Mercury Deposition to a Remote Islet (Pengjiayu) in the Subtropical Northwest Pacific Ocean. *Atmos. Environ.* **2013**, *77*, 474–481.

(47) RSS (Remote Sensing System): Remss. <http://www.remss.com/missions/windsat> (Access date: November 2013).

(48) Sunderland, E. M.; Krabbenhoft, D. P.; Moreau, J. W.; Strode, S. A.; Landing, W. M. Mercury Sources, Distribution, and Bioavailability in the North Pacific Ocean: Insights from Data and Models. *Global Biogeochem. Cycles* **2009**, *23*; Artn Gb2010 doi:.

(49) De Simone, F.; Gencarelli, C. N.; Hedgecock, I. M.; Pirrone, N. Global Atmospheric Cycle of Mercury: A Model Study on the Impact of Oxidation Mechanisms. *Environ. Sci. Pollut. Res.* **2014**, *21*, 4110–4123.

(50) Hong, G.; Heygster, G.; Miao, J. G.; Kunzi, K. Detection of Tropical Deep Convective Clouds from Amsu-B Water Vapor Channels Measurements. *J. Geophys. Res.-Atmos.* **2005**, *110*, (D5).

(51) Nair, U. S.; Wu, Y.; Holmes, C. D.; Ter Schure, A.; Kallos, G.; Walters, J. T. Cloud-Resolving Simulations of Mercury Scavenging and Deposition in Thunderstorms. *Atmos. Chem. Phys.* **2013**, *13* (19), 10143–10157.

(52) Holmes, C. D.; Jacob, D. J.; Corbitt, E. S.; Mao, J.; Yang, X.; Talbot, R.; Slemr, F. Global Atmospheric Model for Mercury Including Oxidation by Bromine Atoms. *Atmos. Chem. Phys.* **2010**, *10* (24), 12037–12057.

(53) Lyman, S. N.; Jaffe, D. A. Formation and Fate of Oxidized Mercury in the Upper Troposphere and Lower Stratosphere. *Nat. Geosci.* **2012**, *5* (2), 114–117.

(54) Wang, Q. Q.; Jacob, D. J.; Spackman, J. R.; Perring, A. E.; Schwarz, J. P.; Moteki, N.; Marais, E. A.; Ge, C.; Wang, J.; Barrett, S. R. H. Global Budget and Radiative Forcing of Black Carbon Aerosol: Constraints from Pole-to-Pole (Hippo) Observations across the Pacific. *J. Geophys. Res.-Atmos.* **2014**, *119* (1), 195–206.

(55) Yuan, J. A.; Houze, R. A. Global Variability of Mesoscale Convective System Anvil Structure from a-Train Satellite Data. *J. Climate* **2010**, *23* (21), 5864–5888.

(56) Fisher, J. A.; Jacob, D. J.; Soerensen, A. L.; Amos, H. M.; Steffen, A.; Sunderland, E. M. Riverine Source of Arctic Ocean Mercury Inferred from Atmospheric Observations. *Nat. Geosci.* **2012**, *5* (7), 499–504.

(57) Soerensen, A. L.; Jacob, D. J.; Streets, D. G.; Witt, M. L. I.; Ebinghaus, R.; Mason, R. P.; Andersson, M.; Sunderland, E. M. Multi-Decadal Decline of Mercury in the North Atlantic Atmosphere Explained by Changing Subsurface Seawater Concentrations. *Geophys. Res. Lett.* **2012**, *39*.

(58) Doi, T.; Tozuka, T.; Yamagata, T. Interannual Variability of the Guinea Dome and Its Possible Link with the Atlantic Meridional Mode. *Clim. Dynam.* **2009**, *33* (7–8), 985–998.

(59) Huete-Ortega, M.; Calvo-Diaz, A.; Grana, R.; Mourino-Carballido, B.; Maranon, E. Effect of Environmental Forcing on the Biomass, Production and Growth Rate of Size-Fractionated Phytoplankton in the Central Atlantic Ocean. *J. Mar. Sys.* **2011**, *88* (2), 203–213.